Investigation into forces on offshore piles with constant and linearly varying diameters using CFD and extended Morison equation under separate wave and current loadings

Kemal Bal, Deniz Bayraktar Bural[*]

Istanbul Technical University, Faculty of Naval Architecture and Ocean Engineering

ARTICLE INFO

ABSTRACT

This study presents a comparative analysis of hydrodynamic forces on cylindrical offshore piles with both constant and linearly varying diameters utilizing computational fluid dynamics (CFD) simulations. The classical Morison equation is evaluated alongside an extended version to address limitations in predicting forces on geometrically complex structures. Mesh convergence studies are performed to select the optimum grid size for separate wave and current simulations. The focus is on test cases characterized by small Keulegan-Carpenter (KC) numbers and relatively high Reynolds (*Re*) numbers within both inertia-dominated and diffraction zones. Numerical simulation results are utilized to compare the force predictions of the classical Morison equation and the extended Morison equation. It is observed that the classical Morison equation performs adequately for constant diameter piles, but it fails to predict forces on variable diameter piles accurately. In contrast, the extended Morison equation, incorporating nonlinear effects and variable cross-sections, provides significantly more accurate force predictions, particularly in the diffraction zone compared to the numerical simulations. This study emphasizes the critical importance of accounting for geometric variations, such as linearly varying pile diameters, under separate waves and currents loadings in hydrodynamic force calculations. These considerations support the development of enhanced design methods and optimization strategies, leading to safer and more efficient offshore structures.

1. Introduction

The behavior of offshore structures, such as piles, under the influence of waves and currents is highly significant for the design and analysis of various marine engineering projects. In general, offshore piles are subjected to complex environmental loads that may affect their structural integrity and stability. Here, waves exert dynamic loads on the piles and cause them to experience cyclic loading, leading to fatigue and potential failure over time. The level of stress and strain the piles experience is determined by the magnitude and frequency of the waves, as well as the characteristics of the pile. On the other hand, currents may induce lateral

---

forces on the piles, causing them to undergo lateral displacements. These forces can be particularly significant in areas with strong tidal or ocean currents [1-2]. To ensure the stability and integrity of offshore piles, engineers must consider the design criteria for wave and current loading, including analyzing environmental conditions, such as wave height, period, direction, and current velocity and direction [3].

The Morison equation [4] is a widely used semi-empirical equation in offshore engineering to estimate the forces exerted on structures, such as piles, by both currents and waves. It has been extensively applied in the design and analysis of offshore structures due to its simplicity and effectiveness. The approach has two basic assumptions: the total wave force is expressed as a superposition of drag and inertia forces while the scattering of waves in the presence of the pile is completely neglected in accord with the Froude-Krylov hypothesis. The final total force is usually formulated using the horizontal component of wave orbital velocity as given by linear theory. However, the application is by no means limited to linear theory. In this study, besides classical Morison equation, a revisited version of Morison equation is adopted where nonlinear effects are included by setting the upper limits of integrals to the actual free surface or wave crest as stated by [5]. On the other hand, the main issue with Morison's equation is the determination of the drag and inertia constants C_d and C_m since comparisons with experimental data and field measurements show considerable scatter [2-6]. Therefore, the drag and inertia coefficients are by no means fixed; hence, the selected values in this study should only be viewed as acceptable choices. However, it is important to note that the Morison equation, in general, is a semi-empirical approach and has certain limitations, which necessitates the use of advanced numerical methods like Computational Fluid Dynamics (CFD) to accurately capture complex effects, such as turbulence, vortex shedding, and nonlinear wave-structure interactions. Ahmed et al. [7] used RANSE to predict solitary wave formation using Ansys-CFX numerically. Similarly, viscous flow around the ship in full scale is also modelled with RANS equations for a transient, incompressible, free surface flow [8]. Wave impact loads on a monopile structure are investigated with a numerical model to study the effect of the shape of breaking waves [9]. Similarly, with RANS equations by employing Star-CCM+, the optimum longitudinal single transverse step location for a high-speed craft has been studied [10] and hydrodynamic performance and energy conversion characteristics of an oscillating buoy has been modeled [11]. Clément et al. [12] evaluated the Morison approach with CFD modeling on surface-piercing cylinders and derived coefficients from CFD loads using OpenFoam. Other than these, REEF3D has been extensively utilized for studying wave-structure interactions in coastal regions [13]. REEF3D uses Reynolds-averaged Navier-Stokes (RANS) equations as well, including the free surface [14] where focused wave kinematics and focused wave–structure interaction is investigated numerically. It is also used to investigate the behavior of structures under wave and current forces [15]. It has also been utilized in high-order discretization schemes and parallel computation strategies to enhance the accuracy and efficiency of wave simulations [16-17]. Kamath et al.[18] investigated the wave interaction with a pair of large tandem cylinders, presenting the changes in diffraction pattern around the cylinder for different wave steepnesses and investigating the differences between theoretical and numerical results for waves with higher steepness. Lin and Liu [17] sought hydrodynamic coefficients induced by waves and currents for submerged circular cylinders. They derived drag and inertia coefficients using simulated wave forces and the least-squares method, providing insights into the hydrodynamic behavior of cylinders. Park and Koo [19] focused on mathematical modeling of partial-porous circular cylinders with water waves. They calculated wave excitation forces and wave run-up on multibodied partial-porous cylinders, highlighting the significant influence of porous-portion ratios and wave conditions on hydrodynamic properties. Song et al. [20] utilized numerical approximation to model water wave interaction with multiple cylinders of arbitrary shape. Their study involved investigating wave run-ups and forces on cylinders using the finite element method, complementing physical model experiments. Zhao et al. [21] derived an analytical solution for the interaction of waves with arrays of circular cylinders. Their work provided a comprehensive understanding of wave forces acting on multiple cylinders by considering incident and scattered wave forces. Wang et al. [22] analyzed the earthquake and wave interaction of circular cylinders considering water-structure-soil interaction. Their results highlighted the substantial increase in dynamic responses of cylinders due to wave forces, emphasizing the importance of considering these forces in structural design.

Ghadirian et al. [23] stated different studies of the wave-current interaction effect on the force coefficients exist from different angles and have different conclusions. However, to our knowledge, cases with

small KC numbers, high Re numbers, and smooth circular cylinders have not been investigated or documented yet. As the diameter of the substructures of offshore wind turbines gets larger, the KC number gets smaller. When the diffraction parameter is high ($\pi D/L$ >1) and the KC number is small, the flow is primarily inertia-dominated, and wave diffraction effects become significant [24]. Koterayama and Hu [25] highlighted the limited research on wave forces on horizontal cylinders at low KC numbers and relatively low Re numbers, noting the complexity of force coefficients under such conditions. Sarpkaya [1] also emphasized the need for further investigation into these specific conditions to improve the understanding of hydrodynamic forces.

The Morison equation is a widely used semi-empirical model for estimating forces on offshore piles; however, it assumes simplified conditions and does not fully account for complex geometries, such as linearly varying diameters. To address these limitations, this study employs an extended version of the Morison equation incorporating nonlinear effects and more complex interactions, enhancing its applicability to modern offshore structures. The effects of wave and current forces on piles with linearly varying diameters have not been extensively studied in the literature. This study uses the CFD module of REEF3D, which solves the Reynolds-averaged Navier-Stokes (RANS) equations, to calculate forces on piles with both constant and linearly varying diameters under four specific conditions characterized by small Keulegan-Carpenter (KC) numbers, small diffraction parameters, and high Reynolds numbers. By comparing results from the classical and extended Morison equations with numerical simulations, this study provides new insights into hydrodynamic forces on these structures, contributing to filling a gap in current research and offering improved methodologies for offshore engineering design.

2. Materials and methods

In this study, the open-source CFD model REEF3D was used to analyze separate wave and current loading interaction with constant and linearly varying bottom-fixed cylinders in a 3D numerical wave tank. For wave-induced cases, the focus is on analyzing forces by small Keulegan-Carpenter (KC) numbers, where the flow around the pile is primarily inertia-dominated rather than governed by viscous forces. The KC number is a dimensionless parameter used to characterize the interaction between wave-induced flow and a structure, such as an offshore pile. The KC number is defined as $KC = \frac{U_m T}{D}$ where U_m is the maximum horizontal velocity of water particles induced by the wave at the pile location, T is the wave period, and D is the characteristic diameter of the pile. For piles with a constant diameter, D refers to the pile's uniform diameter, with values of $D_0 = 0.1\,m$ or $D_0 = 0.8\,m$. For piles with a linearly varying diameter, D refers to D_0, the diameter at still water depth. In these cases, the values used for D_0 are 0.066 m or 0.53 m, depending on the specific pile geometry.

Before starting numerical simulations, mesh convergence studies were conducted. As shown in Figure 1, the Morison equation is used for the validation of wave forces and physical experiments by Aksel et al. [26] are used to validate the current forces. Here, two test scenarios considering waves and currents are created for mesh convergence. In the first test scenario, waves acting on two different constant diameter cylinders are investigated, and numerical wave forces for various grid sizes are compared with the results of the classical Morison equation to select the optimal grid size. In the second test scenario, current effects are compared with the results of physical experiments [26], leading to the selection of the optimal mesh grid size. After mesh convergence and verification tests, eight cases are set up and grouped by their geometry (two piles with different constant diameters – T1R1 and T1R2, and two different piles with linearly varying diameters – T2R3 and T2R4). The summary of these cases for different pile types and associated wave and current conditions is given in Table 1.

Table 1 Summary of numerical cases for different pile types and associated wave and current conditions

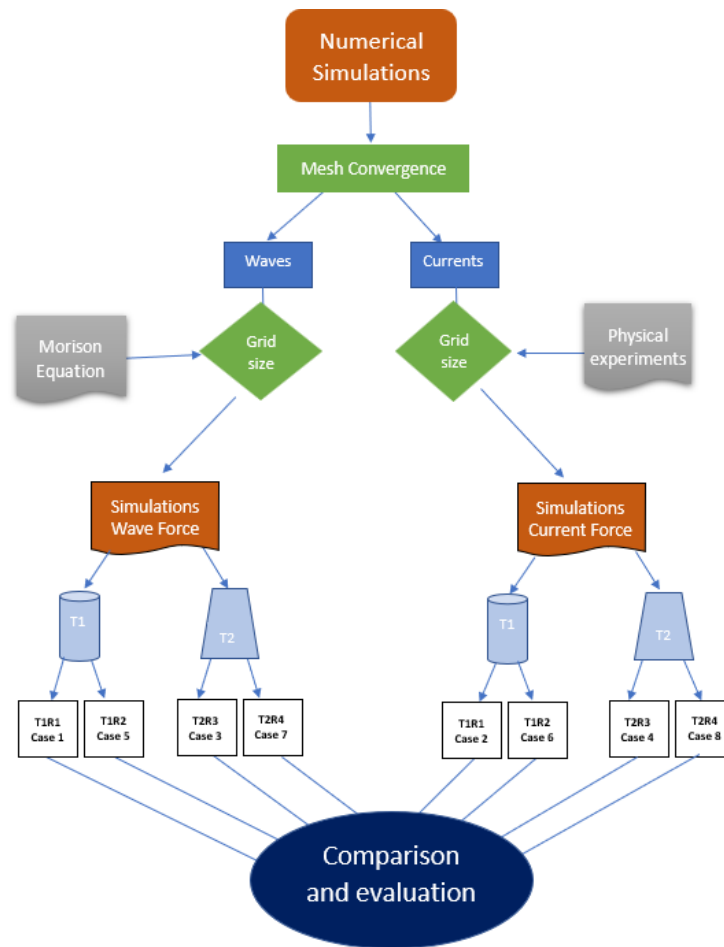| Pile Type	Cases	Pile Diameter(s) [m]	Wave Height [m]	Wave Period [s]	Current [m/s]
T1R1	Case 1	D_0=0.1	0.021	1.98	-
	Case 2	D_0=0.1	-	-	0.33
T2R3	Case 3	D_0=0.066 D_h=0.132	0.021	1.98	-
	Case 4	D_0=0.066 D_h=0.132	-	-	0.33
T1R2	Case 5	D_0=0.8	0.021	1.98	-
	Case 6	D_0=0.8	-	-	0.33
T2R4	Case 7	D_0=0.53 D_h=1.07	0.021	1.98	-
	Case 8	D_0=0.53 D_h=1.07	-	-	0.33

Fig. 1 Methodology for analyzing wave and current forces using REEF3D

T1R1 and T2R3 are in the zone where inertia is dominant, while T1R2 and T2R4 are in the diffraction zone. Each of them is tested with separate waves and currents loading. Thus, separate wave and current forces acting on cylinders with constant and linearly varying diameters are examined in both diffraction and inertia dominant zones. In all eight cases mentioned in Table 1, numerical forces induced by separate waves and currents are compared with the results of classical Morison and Morison Equation revisited by Beji [5] as seen in Figure 1. It should be noted that for T1R1-Case 1 and T2R3-Case 3 the drag coefficient C_d is 0.7 and the inertia coefficient C_m is 2.06. For T1R2-Case 5 and T2R4-Case 7, these values are 0.7 and 1.74, respectively.

2.1 Morison equation

The Morison equation is a fundamental tool used in offshore engineering to estimate the hydrodynamic forces exerted by waves and currents on cylindrical structures. Beji [5] extended the Morison equation to include nonlinear effects and more complex interactions, enhancing its applicability to constant and linearly varying diameter piles.

2.1.1   Application for Constant Diameter Circular Pile

For constant diameter circular cylinders, the Morison equation is expressed as:

$$dF = \frac{1}{2}\rho C_d |U|U dA_p + \rho C_m \frac{dU}{dt} d\forall \tag{1}$$

In Equation 1, the total infinitesimal force dF acting on the infinitesimal height dz of the pile is given by the expression where ρ is the fluid density, U is the horizontal flow velocity, dA_p is the infinitesimal projected frontal area, $d\forall$ is the infinitesimal displaced volume of the circular structure, C_d is the dimensionless constant coefficient of drag, and C_m is the dimensionless constant coefficient of inertia (mass).

This classical Morison formulation, as shown in Figure 2, assumes that the diameter of the cylinder is constant along its length and that the cylinder is fully submerged. While this equation provides a reasonable approximation of the forces acting on such structures, it is limited in its application to modern offshore structures that often have more complex geometries.
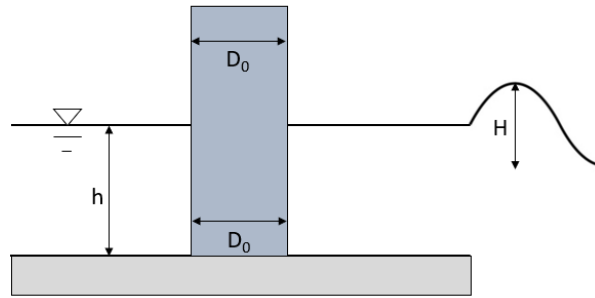

Fig. 2 Constant diameter circular pile parameters

Equations (2) to (8) are derived from Beji [5], which describe the drag and inertia forces for a cylindrical pile using the Morison equation and provide conditions for determining the maximum force. The drag and inertia forces of the Morison equation for a fixed diameter cylindrical pile are expressed as $F_d = F_{d0}\bar{F}_d$ and $F_i = F_{i0}\bar{F}_i$. Here, horizontal drag and inertia force components F_d and F_i are given in Equation 2.

$$F_{d0} = \frac{\frac{1}{2}\rho g C_d D_0 H^2}{8 \sinh 2\mu_h} \; ; \; F_{i0} = \frac{\frac{\pi}{4}\rho g C_m D_0^2 H}{2 \cosh \mu_h} \tag{2}$$

The non-dimensional drag and inertia force components $\bar{F}_d$ and $\bar{F}_i$ are given as;

$$\bar{F}_d = 2\mu_h(1 + \varepsilon_h) + \sinh 2\mu_h(1 + \varepsilon_h) \tag{3}$$

$$\bar{F}_i = \sinh \mu_h(1 + \varepsilon_h) \tag{4}$$

In equations 3 and 4, the nonlinearity parameter is $\varepsilon_h = a/h$ and dispersion parameter is $\mu_h = kh$. The linearized forms of non-dimensional force and moment components are obtained by simply setting the nonlinearity parameter ε_h to zero, where subscript l refers to linearization as denoted by Equations 5 and 6.

$$\bar{F}_{dl} = 2\mu_h + \sinh 2\mu_h \tag{5}$$

$$\bar{F}_{il} = \sinh \mu_h \tag{6}$$

To find the maximum force, F_i and F_d values should be compared and the maximum force should be determined according to the following condition given in Equation 7.

$$\frac{F_i}{2F_d} \leq 1 \tag{7}$$

If this condition is met, the maximum force is calculated as in Equation 8.

$$F_{max} = F_d + \frac{F_i^2}{4F_d} \tag{8}$$

If $F_i/2F_d \geq 1$ then maximum force is $F_{max} = \pm F_i$.

2.1.2 Application for linearly varying diameter circular pile

The classical Morison equation is revisited by Beji [5] to extend its applicability to circular piles with linearly varying diameters as depicted in Figure 3. This extension helps predict the hydrodynamic forces on structures with non-uniform geometries, common in contemporary offshore engineering.
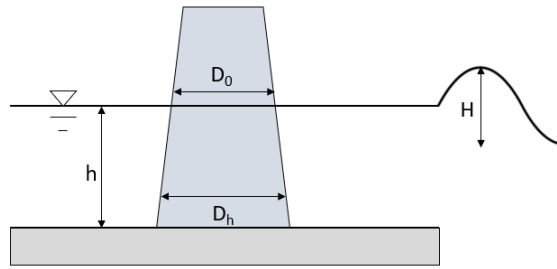

Fig. 3 Linearly varying diameter circular pile parameters

For a cylinder with a linearly varying diameter defined as $D(z) = D_0(1 - r_h z/h)$ where $r_h = D_h/D_0 - 1$ the force components are modified to account for the varying geometry.

The extended Morison equation for such cylinders incorporates the integration of pressure and shear stress over the surface area of the structure, leading to the following formulations for the drag and inertia forces, as given in Equations 9 and 10.

$$\bar{F}_d = 2\mu_h(1 + \varepsilon_h)\left[1 + \frac{r_h(1-\varepsilon_h)}{2}\right] + (1 - r_h\varepsilon_h)\sinh 2\mu_h(1 + \varepsilon_h)$$

$$- \left(\frac{r_h}{2\mu_h}\right)[1 - \cosh 2\mu_h(1 + \varepsilon_h)] \tag{9}$$

$$\bar{F}_i = [(1 - r_h\varepsilon_h)^2 + 2r_h^2/\mu_h^2]\sinh \mu_h(1 + \varepsilon_h)$$

$$- (2r_h/\mu_h)[(1 + r_h) - (1 - r_h\varepsilon_h)\cosh \mu_h(1 + \varepsilon_h)] \tag{10}$$

Linearized forms are given in Equations 11 and 12.

$$\bar{F}_{dl} = 2\mu_h(1 + r_h/2) + \sinh 2\mu_h - (r_h/2\mu_h)(1 - \cosh 2\mu_h) \tag{11}$$

$$\bar{F}_{il} = (1 + 2r_h^2/\mu_h^2)\sinh \mu_h - (2r_h/\mu_h)(1 + r_h - \cosh \mu_h) \tag{12}$$

For circular piles with varying diameters, an extension of the Morison equation significantly improves the accuracy of force predictions. This improvement is particularly important under complex wave conditions, where the classical Morison equation falls short. By integrating the pressure and shear stress over the variable surface area, the extended Morison equation provides a more accurate and reliable estimate of the hydrodynamic forces acting on these structures.

2.2 Numerical model

Numerical simulations are demonstrated by REEF3D where it has been extensively utilized for studying wave-structure interactions in coastal regions [13]. It employs the Reynolds-Averaged Navier-Stokes (RANS) equations to simulate flow dynamics, including the free surface evolution [15]. It has been applied in various studies to investigate the behavior of structures under wave and current forces. It utilizes high-order discretization schemes and parallel computation strategies to enhance the accuracy and efficiency of wave simulations [16]. The RANS equations form the basis of the REEF3D::CFD module, which is the part of the REEF3D software that handles fluid dynamics, allowing for precise simulations of how incompressible fluids behave around structures and the resulting forces. The application of REEF3D in this study focused on analysing the wave and current forces on circular cylinders with both constant and varying diameters.

Continuity and momentum equations are shown in Equations 13 and 14.

$$\frac{\partial \rho}{\partial t} + \nabla \cdot (\rho \boldsymbol{u}) = 0 \tag{13}$$

$$\frac{\partial \rho \boldsymbol{u}}{\partial t} + \nabla \cdot (\rho \boldsymbol{u}\boldsymbol{u}) = -\nabla p + \nabla \cdot \tau \tag{14}$$

where ρ is the fluid density, $\boldsymbol{u}$ is the velocity vector, p is the pressure, τ represents the stress tensor, incorporating both viscous and Reynolds stresses.

To simulate turbulent flows, k-ε model has been used, as given in Equations 15 and 16. This model includes two transport equations: one for the turbulence kinetic energy k and another for its dissipation rate ϵ:

$$\frac{\partial k}{\partial t} + u \cdot \nabla k = \nabla \cdot (\nu_t \nabla k) + P_k - \epsilon \tag{15}$$

$$\frac{\partial \epsilon}{\partial t} + u \cdot \nabla \epsilon = \nabla \cdot (\nu_t \nabla \epsilon) + C_{1\epsilon} \frac{\epsilon}{k} P_k - C_{2\epsilon} \frac{\epsilon^2}{k} \tag{16}$$

where ν_t is the turbulent viscosity, P_k the production term of turbulence kinetic energy, $C_{1\epsilon}$ and $C_{2\epsilon}$ are model constants.

The Volume of Fluid (VOF) method is used to track the free surface between fluids. The advection equation is given in Equation 17.

$$\frac{\partial F}{\partial t} + \boldsymbol{u} \cdot \nabla F = 0 \tag{17}$$

where F represents the volume fraction of fluid.

Calculating wave forces on structures involves integrating pressure and shear stresses exerted by the waves on the structure' surface. The forces acting on a structure are derived from the integration of pressure and shear stress over the surface area of the structure. The total wave force F_w is computed as in Equation 18:

$$F_w = \int_{\partial V} (-pn + \tau) \, dA \tag{18}$$

where p is the pressure exerted by the wave, n is the unit normal vector to the surface, τ is the shear stress vector, ∂V represents the surface area of the structure. The pressure force F_p is calculated by integrating the pressure over the surface area of the structure:

$$F_p = \int_{\partial V} -pn \, dA \tag{19}$$

This force given in Equation 19 represents the normal component of the wave force acting perpendicular to the surface. The shear stress force F_τ, given in Equation 20, is computed by integrating the shear stress over the surface area of the structure:

$$F_\tau = \int_{\partial V} \tau \, dA \tag{20}$$

This force represents the tangential component of the wave force acting parallel to the surface. The total wave force acting on the structure is the sum of the pressure force and the shear stress force; $F_w = F_p + F_\tau$.

3.   Mesh convergence for separate wave and current loads acting on constant diameter circular piles

Mesh convergence is crucial as it ensures that the numerical solution becomes independent of the grid size, leading to accurate and stable results. Different grid sizes are tested to ensure the accuracy and reliability of the numerical simulations. The process of mesh convergence is performed to determine the optimal grid size for simulating wave forces in regular waves, with comparisons made using wave forces obtained from the classical Morison equation. Additionally, a mesh convergence test is conducted for current flow velocities by comparing the results with the experimental findings of [26] with flow data measured at a distance of 4D. In the grid independence studies, a grid stretching factor of 1.2 is employed to control the mesh size within the computational domain. For wave cases, it is found that a finer mesh with an initial grid size of 0.01 around the pile provided the best agreement with the classical Morison equation's wave force results. For current cases, a finer mesh with an initial grid size of 0.025 around the pile provided the best agreement with the experimental findings of [26]. This approach allowed for a smooth transition to a coarser grid in the far field, optimizing computational efficiency while maintaining the necessary accuracy near the pile.

3.1 Wave acting on a constant diameter pile

Considering waves only, a mesh convergence study is conducted for piles with two different constant diameters: T1R1-Case 1 and T1R2-Case 5. The domain dimensions are set as follows: width = 1.5 m, length = 20 m, and height = 1 m. A screenshot of waves acting on a constant diameter pile is given in Figure 4a. The piles in both case 1 and case 2 are positioned at 12 meters from the inlet, as given in Figure 4b. Figure 4c illustrates mesh refinement and grid stretching along the flow direction.
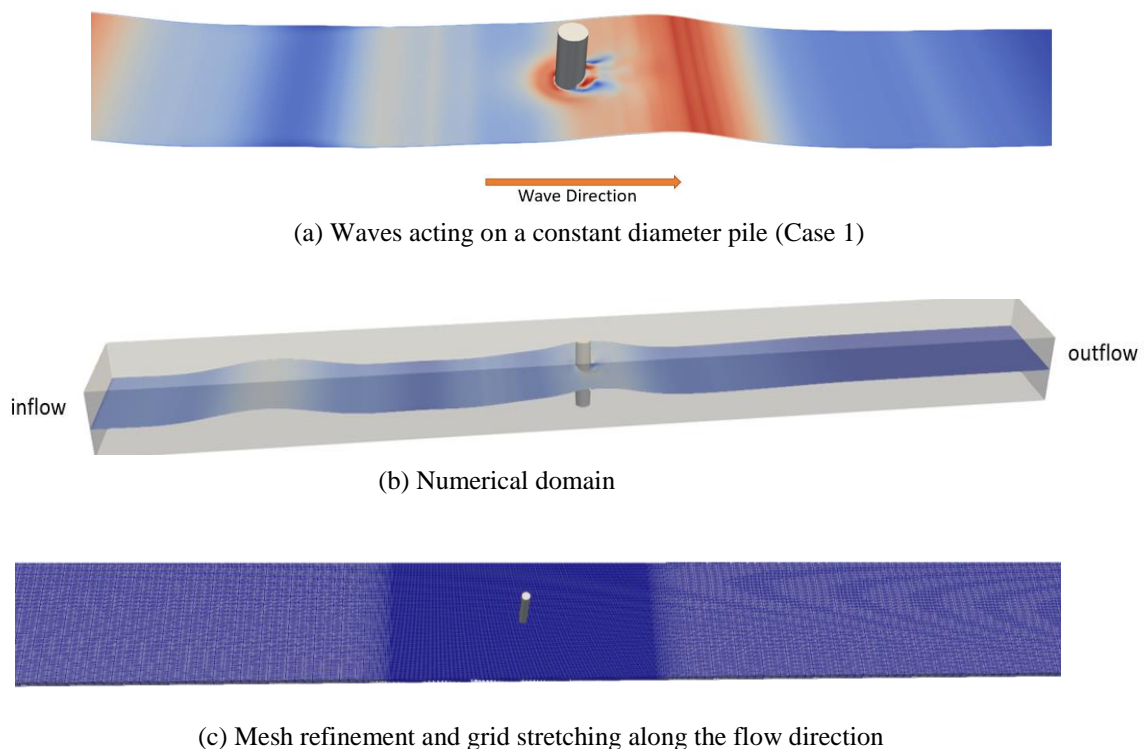

Wave Direction

(a) Waves acting on a constant diameter pile (Case 1)

inflow   outflow

(b) Numerical domain

(c) Mesh refinement and grid stretching along the flow direction

Fig. 4 Numerical setup and wave interaction with a constant diameter pile for Case 1

This study involved testing three different grid sizes (0.10, 0.050, and 0.01). The convergence tests are conducted with wave conditions specified in Table 1 acting on T1R1-Case 1 and T1R2-Case 5. In Figures 5a and 5b, the grid size convergence can be seen respectively for both cases.
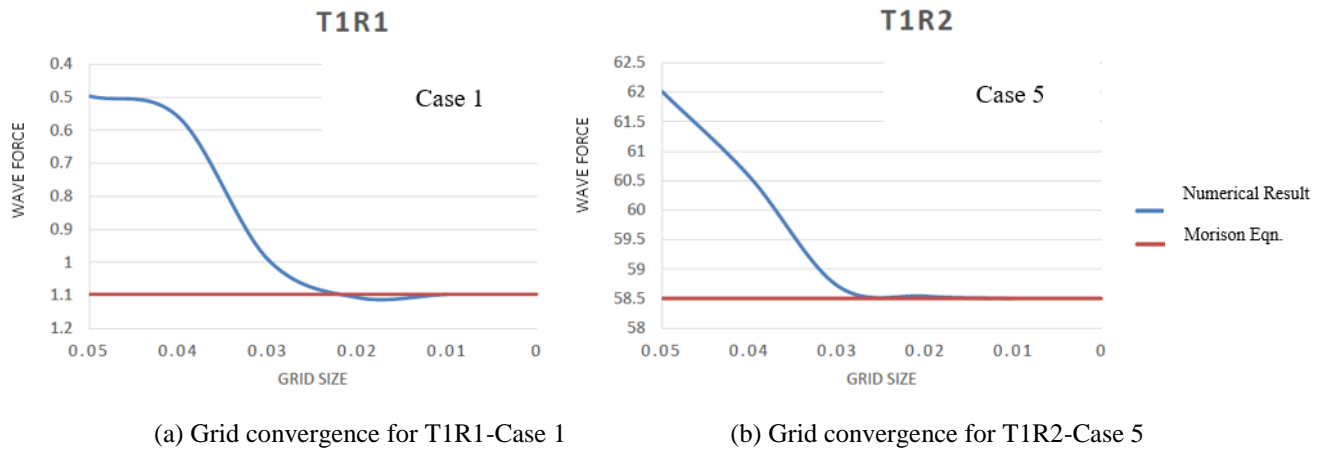

(a) Grid convergence for T1R1-Case 1   (b) Grid convergence for T1R2-Case 5

Fig. 5 Comparison of numerical wave force (blue line) and wave force obtained using classical Morison equation (red line) for cases T1R1-Case 1 and T1R2-Case 5 as a function of grid size

The wave force results (blue line) obtained from these tests are compared with the results obtained using the classical Morison equation (red line) to validate the numerical simulations for cases T1R1-Case 1 and T1R2-Case 5, as given in Figures 5a and 5b, respectively. As the mesh size is refined, the results converge towards those predicted by the classical Morison equation. The convergence is evident as the mesh size decreased to 0.01 m, with minimal differences observed. However, it is important to note that the convergence tests rely on classical Morison equation solutions, and the diffraction zone may not yield the best results due to the limitations of the Morison equation in capturing diffraction effects. As the mesh refines, wave force begins to converge to the results of the classical Morison equation. This convergence starts to give almost the same result when the mesh size is 0.01m. The mesh convergence study confirmed that the grid size of 0.01 m is appropriate for the set-up, ensuring that the numerical results are independent of grid resolution.

The wave force results (blue line) obtained from these tests are compared with the results obtained using the classical Morison equation (red line) to validate the numerical simulations for cases T1R1-Case 1 and T1R2-Case 5, as given in Figures 5a and 5b, respectively. As the mesh size is refined, the results converge towards those predicted by the classical Morison equation. The convergence is evident as the mesh size decreased to 0.01 m, with minimal differences observed. However, it is important to note that the convergence tests rely on classical Morison equation solutions, and the diffraction zone may not yield the best results due to the limitations of the Morison equation in capturing diffraction effects. As the mesh refines, wave force begins to converge to the results of the classical Morison equation. This convergence starts to give almost the same result when the mesh size is 0.01m. The mesh convergence study confirmed that the grid size of 0.01 m is appropriate for the set-up, ensuring that the numerical results are independent of grid resolution.

3.2 Current acting on a constant diameter pile

Considering currents only, the mesh convergence study is conducted by replicating the experimental set-up of Aksel et al. [26]. The pile used in these set of experiments is modeled to investigate the current acting on it as seen in Figure 6 from both top and side views.
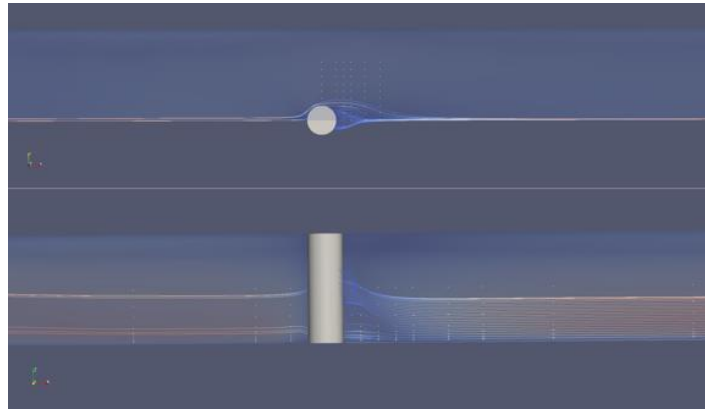
Fig. 6 Currents acting on the constant diameter circular pile

In the physical experiment, the pile diameter D is 0.16 m and U is the free flow velocity, 0.33 m/s. Water depth is 0.32 m, channel length is 10 m, and the pile is located 2 m away from the inlet. In the experimental study, the velocity measurement grid applied by [27] had been used, as seen in Figure 7a. This grid comprises thirteen locations in the longitudinal direction and nine points depthwise. Figure 7b illustrates the numerical replication of this physical experiment depicted in Figure 7a, where dots represent the measurement points. A comprehensive validation of all experimental results is conducted for all measurement points; however, the detailed results are not presented in this text.
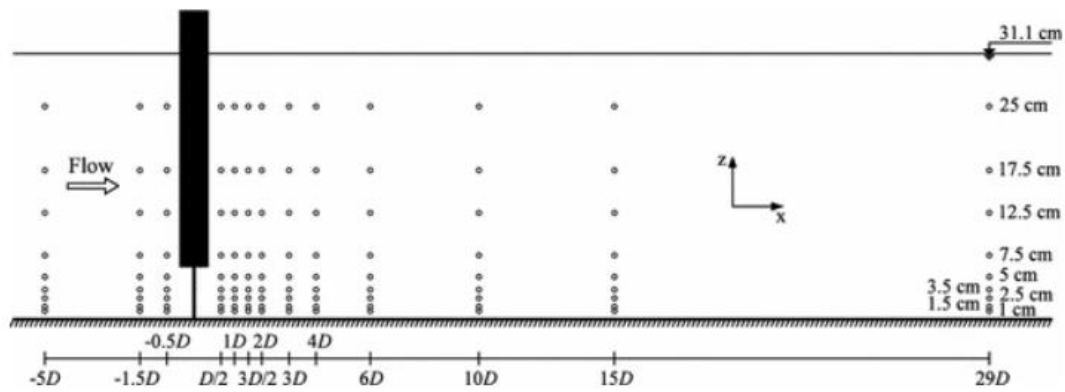

(a) Physical experiment and probe locations [27]; vertical (x–z) plane at the centerline ($y/D = 0$)
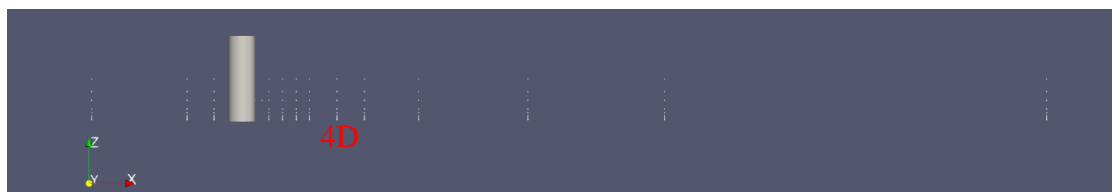
(b) Numerical replication of the physical experiment

Fig. 7 Physical experiment setup and its numerical replication for current-induced velocity profiles

The mesh convergence study is conducted using three different grid sizes (0.10, 0.050, and 0.025), as shown in Figures 8a, 8b, and 8c, respectively. Here, dots show the experimental results at a 4D distance, and the red line shows the numerical results at that point. For each grid size, flow velocities at a distance of 4D are computed. These results are compared with the experimental data measured at the same 4D distance, indicated by Figures 7a and 7b. The mesh convergence study for current acting on a constant diameter circular cylinder, using grid sizes 0.10, 0.050, and 0.025, identified 0.025 as the optimal grid size (Figure 8c), ensuring numerical solution independence from grid resolution. This grid size provided the most reliable and accurate results, as seen in the strong correlation between numerical and experimental profiles at most probe locations in Figure 8c.
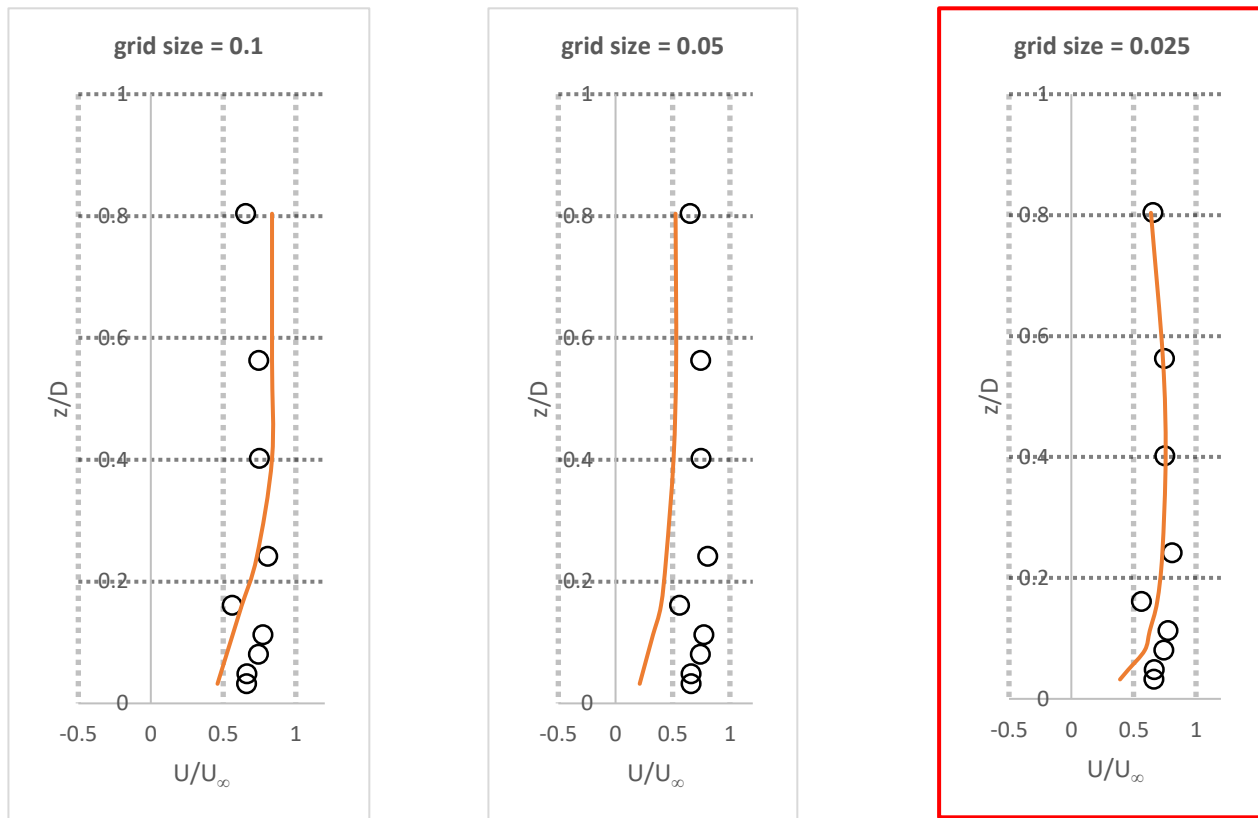
(a) Current case mesh convergence study (grid size=0.1)

(b) Current case mesh convergence study (grid size=0.05)

(c) Current case mesh convergence study (grid size=0.025)

—— Numerical Model Results   ◯ Experimental Results

Fig. 8 Mesh convergence study for current case velocity profiles, comparing numerical model results (orange solid line) with experimental results (black circles) for different grid sizes

4. Simulation of separate wave and current acting on circular piles

This study focused on examining two types of circular piles; piles with constant diameters (T1R1 and T1R2) as seen in Figure 9a and piles with linearly varying diameters (T2R1 and T2R2) as seen in Figure 9b.
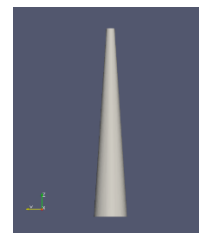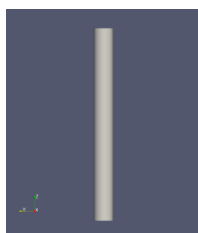
(a) Constant diameter piles - T2R1 and T2R2   (b) Linearly varying diameter piles - T2R1 and T2R2

Fig. 9 Types of constant and linearly varying diameter piles examined under separate wave and current loadings

In total, eight scenarios summarized in Table 1 are created to numerically calculate the separate wave and current forces acting on them. The numerical wave and current forces acting on each type of piles are then compared with the results of the classical Morison equation and extended Morison equation, as given by Beji [5].

4.1 Numerical set-up

In all wave cases, the water depth is 0.5 m. Domain width is 1.5 m and length is 20 m. Piles T1R1-Case 1, T2R3-Case 3, T1R2-Case 5 and T2R4-Case 7 are positioned 12 meters from the inlet. In all current cases the water depth is 0.32 m. Domain width is 1.5 m and length is 10 m. Piles T1R1-Case 2, T2R3-Case 2, T1R2-Case 6 and T2R4-Case 8 are positioned 2 meters from the inlet. Table 1 shows all the cases and their characteristics. In cases 1 and 2, the diameter is 0.1 meters and in cases 3 and 4, the diameter is 0.066 meters at still water depth and 0.132 meters at the bottom. In cases 5 and 6, the diameter is 0.8 meters, and in cases 7 and 8, the diameter is 0.53 meters at still water depth and 1.07 meters at the bottom. The wave height for all cases is 0.021 m, and the wave period is 1.98 s. For all current cases (cases 2, 4,6 and 8), the current flow is 0.33 m/s.

The investigation into wave cases (Cases 1, 3, 5, and 7) presented in Table 1 aims to analyse the impact of diffraction. Cases 1 and 3 are specifically chosen to reside within Zone I, marked by the red dot in Figure 10, where inertia effects are dominant.
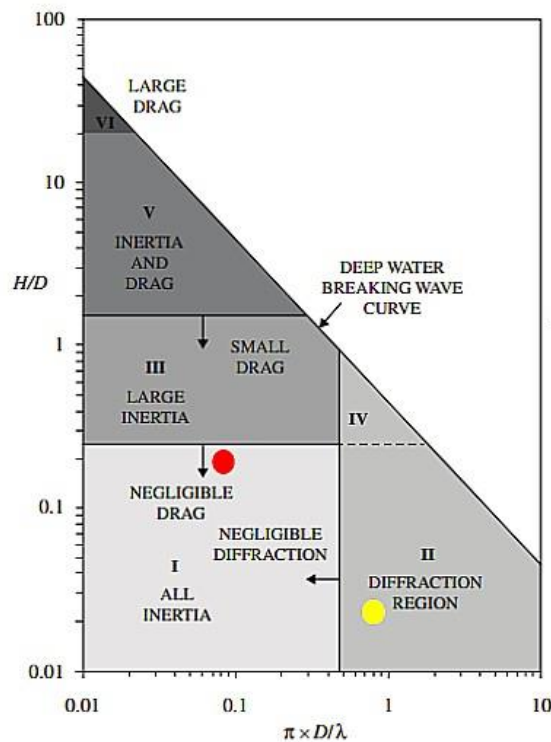

Fig. 10 Morison equation and diffraction relationship [2]; red dot: Cases 1-3, yellow dot: Cases 5-7

Conversely, cases 5 and 7, marked by the yellow dot in Figure 10, are deliberately placed within Zone 2, where diffraction takes place. This selection evaluates the reliability of the Morison equation by comparing its predictions with those of direct numerical simulations.

4.2 Calculation of Wave and Current Forces

The total hydrodynamic force F_T acting on the surface of the pile due to waves and currents is determined by integrating the effects of pressure and shear stress over the pile's surface, Γ, as shown in Equation 21:

$$F_T = \int_\Gamma (-np + n \cdot \tau) d\Gamma \tag{21}$$

This approach involves a numerical calculation where the model accurately captures the surface profile of the pile, allowing for precise computation of the pressure distribution around the cylinder. In this method, both pressure (p) and shear stress (τ) are calculated along the boundary of the pile, and their effects are integrated to determine the forces exerted by the fluid. The unit normal vector n is defined as pointing outward from the pile's surface, indicating the direction in which the pressure acts perpendicular to the surface. The

term $-np$ represents the force due to pressure acting inward against the pile surface. The term $n \cdot \tau$ represents the dot product of the normal vector n with the shear stress vector τ, yielding the scalar component of the shear stress that aligns with the normal direction. By integrating these contributions over the surface Γ, the equation accounts for both normal pressure forces and shear stress components, providing a comprehensive measure of the hydrodynamic forces. This method ensures that the pressure and shear stresses are accurately represented and summed over the pile's surface, yielding a robust evaluation of the fluid-structure interactions under varying wave and current conditions.

5. Numerical results

A comprehensive analysis of wave and current forces acting on circular piles with both constant and varying diameters is presented using numerical simulations (REEF3D), the classical Morison Equation, and a revisited version by Beji [5]. The results show that the classical Morison equation performs well for constant diameter piles but has limitations for linearly varying diameter structures. The Reynolds number analysis highlights that cases close to the transitional regime (e.g., T2R3) show more significant deviations, while those in the turbulent regime (e.g., T1R2 and T2R4) demonstrate better alignment with numerical results. This comprehensive analysis underscores the significance of considering geometric variations and flow regimes in hydrodynamic force calculations.

Investigating separate wave and current cases involves analysing the impact of diffraction and inertia effects on piles with different geometries. Based on Figure 10, Cases 1, 2, 3, and 4 are located in Zone I (Inertia Dominated). This zone is characterized by large inertia forces with relatively small drag. Cases 5, 6, 7, and 8 fall into Zone II (Diffraction Region), where wave diffraction effects become significant, and the interaction is more complex. The revised Morison equation offers improved accuracy, particularly in the diffraction zone where complex flow interactions occur.

Wave cases (1, 3, 5, 7) examine the influence of diffraction on wave forces. With the force results obtained from CFD simulations, these scenarios are compared with those obtained using the classical and extended Morison equations. Current cases (2, 4, 6, 8) focus on current-induced forces and their comparison with the Morison equation. Wave and current conditions are specific to each case, as summarized in Table 1. Table 2 provides a detailed comparison of wave force results from numerical simulations and predictions from both Morison equations for different pile geometries. In Table 2, the error percentages between the numerical force calculations and the Morison equations range from 2.7% to 9.38% for Beji (2019) and 4.59% to 8.41% for the classical Morison method. These values indicate that while both approaches are reasonably close to the numerical results, noticeable variations depend on the specific pile type and wave case considered. This also underscores the importance of grid refinement to accurately capture the forces, especially in complex flow conditions.

In the inertia-dominated regime (Zone I), the KC numbers of T1R1 Case 1 and T2R3 Case 3 are 1 and 1.52. While the Reynolds (Re) numbers for these cases are close to the transitional flow regime, the numerical model effectively captures the inertia effects. This effective capture is reflected in the close agreement between numerical simulations and semi-empirical predictions. T1R1 Case 1, the numerical force is 1.09 N, closely matching Beji (2019)'s 1.12 N and Classical Morison's 1.14 N. This agreement highlights the accuracy of numerical simulations and empirical models in the inertia-dominated zone. Similarly, T2R3 Case 3, which is also in Zone I, shows good agreement with numerical and semi-empirical predictions, with a numerical force of 1.07 N compared to Beji (2019)'s 1.17 N and Classical Morison's 1.16 N, underscoring the reliability of these models in this zone as well.

In Zone II, significant differences arise. KC numbers of T1R2 Case 5 and T2R4 Case 7 are smaller than 1, and Re numbers indicate a turbulent regime. For T1R2 Case 5, the numerical force is 58.95 N, whereas Beji (2019) predicts 60.54 N, and the Classical Morison equation gives 61.87 N. These discrepancies highlight the limitations of the classical Morison Equation in capturing complex interactions in the diffraction zone. T2R4 Case 7 also shows deviations with a numerical force of 59.30 N compared to Beji's (2019) 64.86 N and the Classical Morison's 64.26 N, reinforcing the need for advanced modeling techniques. In these cases, the KC

numbers are lower, and the Reynolds numbers indicate turbulent flow, making accurate modeling more challenging with classical Morison Equations but necessary to capture the diffraction effects.

Table 2 Comparative analysis of numerical wave force results with Morison equation predictions for different pile geometries.

Pile Type	Case	Wave	Numerical Force [N]	Morison by Beji (2019) [N]	Classical Morison [N]
T1R1	Case 1	+	1.09	1.12	1.14
T2R3	Case 3	+	1.07	1.17	1.16
T1R2	Case 5	+	58.95	60.54	61.87
T2R4	Case 7	+	59.30	64.86	64.26

Figures 11 to 14 further illustrate these wave force results, comparing the numerical model against both Morison equations for various pile geometries under wave conditions. The comparison of Figures 11 to 14 highlights the impact of flow regime and geometric characteristics on wave force predictions.
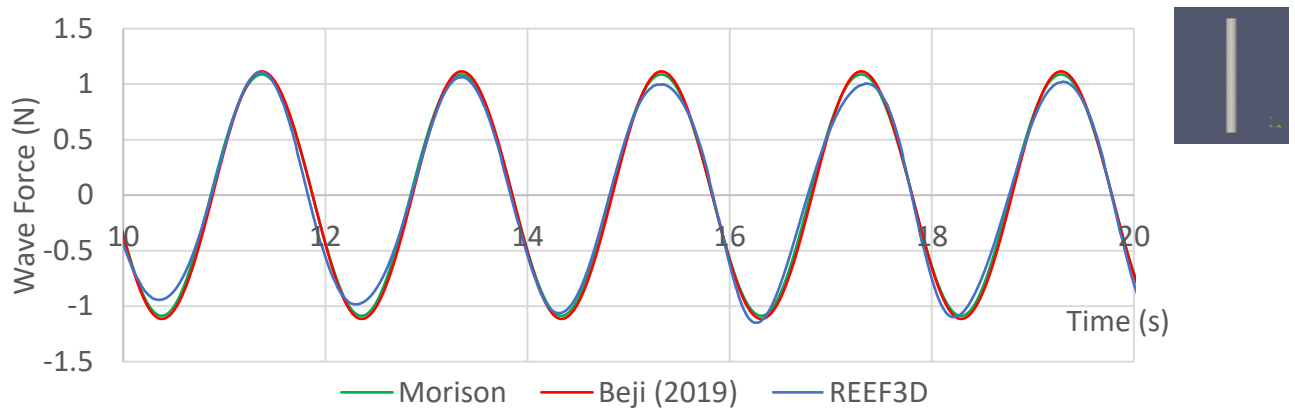

Fig. 11 T1R1-Case 1 KC=1 *Re*= 5208 wave force results

Figures 11 and 12 (T1R1-Case 1 and T2R3-Case 3) involve Reynolds numbers close to the transitional regime, where the flow exhibits both laminar and turbulent characteristics, complicating accurate wave force modeling. In these cases, while numerical results and Beji (2019) provide closely aligned predictions, the Classical Morison equation tends to overestimate wave forces, particularly for linearly varying diameters, as seen in Figure 12, indicating its limitations in transitional flows. In Figure 11, the wave force results from numerical simulations and Beji (2019) show excellent agreement with each other and the Classical Morison equation, indicating robustness in capturing inertia effects for constant diameter piles. However, in Figure 12, the results from numerical simulations show noticeable differences compared to both the Classical Morison equation and Beji (2019). This discrepancy can be attributed to REEF3D's ability to more accurately capture the detailed flow dynamics and turbulence effects in transitional regimes.
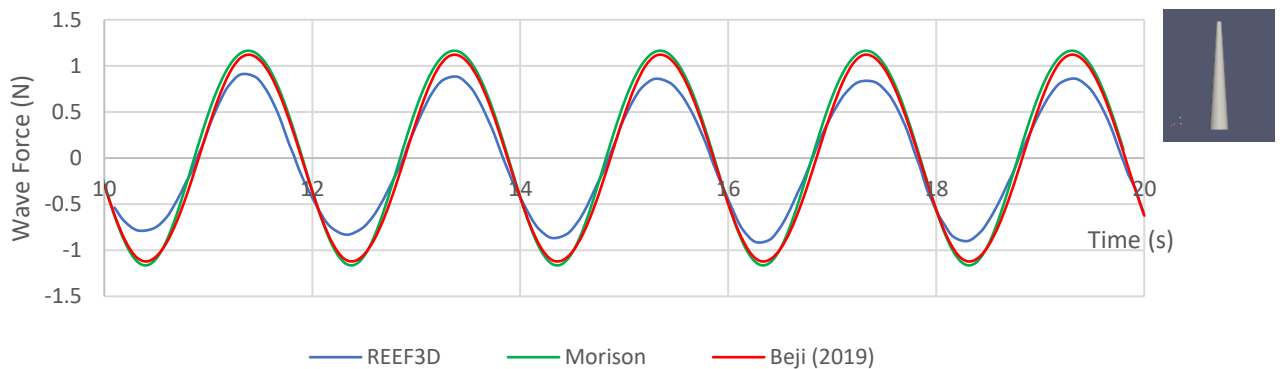

Fig. 12 T2R3-Case 3 KC=1.52 *Re*= 3437 wave force results

14

In contrast, Figures 13 and 14 (T1R2-Case 5 and T2R4-Case 7) involve turbulent Reynolds numbers where the flow is fully turbulent and chaotic yet statistically predictable. Here, predictions from numerical simulations, Beji (2019) and the Classical Morison equation show better agreement, as the turbulent regime reduces sensitivity to specific geometric details, allowing the Classical Morison equation to approximate forces more accurately even for piles with linearly varying diameters like in Figure 14.

In Figure 13 (T1R2-Case 5), which falls into Zone II (Diffraction Zone), the results from numerical simulations, Beji (2019) and the Classical Morison equation show good agreement, indicating that all models can accurately capture the wave forces for constant diameter piles in the turbulent regime. The chaotic yet statistically predictable nature of turbulent flows allows for reasonable accuracy with semi-empirical models, demonstrating that the Classical Morison equation can still be effective in such scenarios despite its simplifications. This contrasts with the transitional regime seen in Figure 12, where the numerical results differ significantly from both the Classical Morison equation and Beji (2019) due to the complexities of transitional flows and geometric variations. This difference highlights the importance of advanced numerical methods like REEF3D in capturing detailed flow dynamics in transitional regimes, whereas in fully turbulent regimes, even simplified semi-empirical models can provide reasonable predictions.
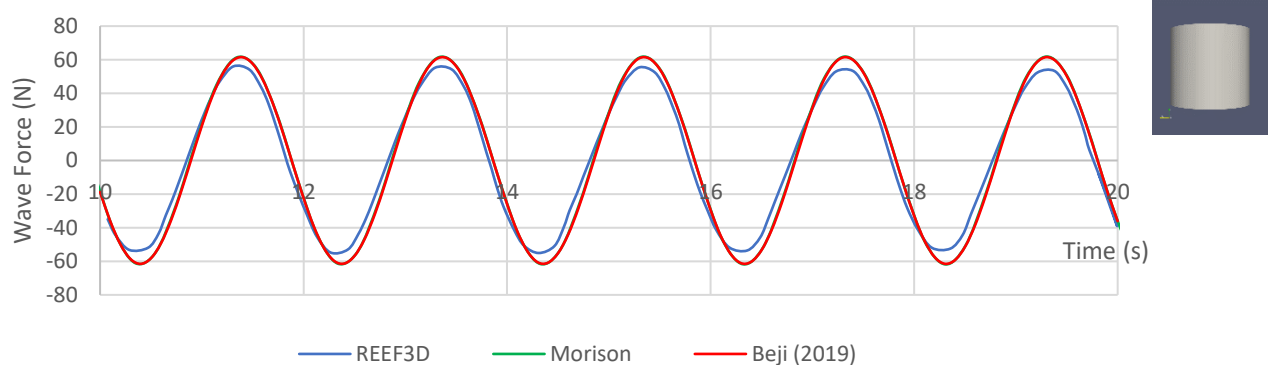

Fig. 13 T1R2-Case 5 KC=0.13 *Re*= 41663 wave force results

In Figure 14 (T2R4-Case 7), the results from numerical simulations and Beji (2019) show good agreement, indicating their suitability for capturing the complex wave-structure interactions in the diffraction zone. Despite the linearly varying diameter and higher Reynolds numbers, the Classical Morison equation also provides reasonable predictions. This suggests that in the turbulent regime, where the flow is chaotic but statistically predictable, the Classical Morison equation can still offer reasonable accuracy. The overall agreement across the models demonstrates their effectiveness in the turbulent regime, emphasizing the importance of considering flow characteristics and geometric complexities in wave force predictions.
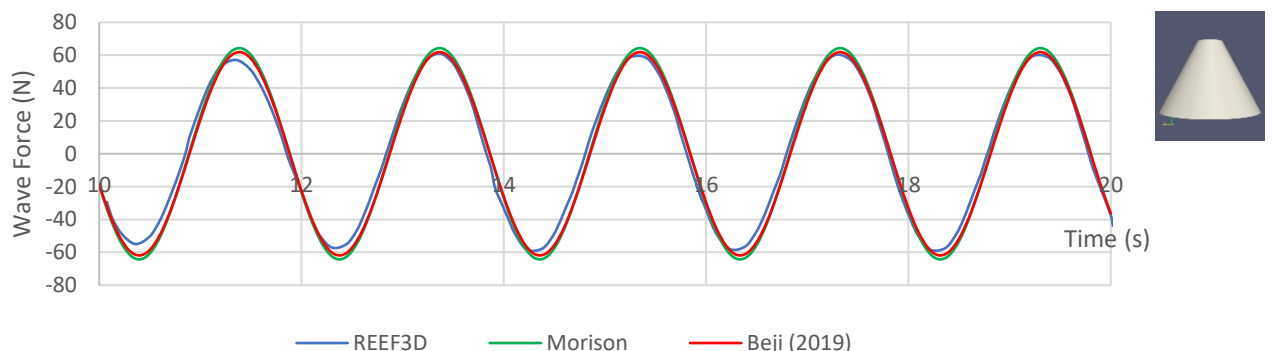

Fig. 14 T2R4-Case 7 KC=0.19 *Re*= 27601 wave force results

The sensitivity to geometric variations is evident; constant diameter piles (Figures 11 and 13) show good agreement across models in both regimes, while linearly varying diameters (Figures 12 and 14) exhibit significant performance variations. Close to transitional regimes, the Classical Morison equation's

15

simplifications are less effective, leading to discrepancies, whereas in turbulent regimes, the chaotic but predictable nature allows better performance. The classification into Zone II (Diffraction Zone) and Zone I highlights the importance of flow regime in wave-structure interaction modeling; in Zone I (inertia-dominated), precise geometric modeling is crucial for accuracy, captured better by numerical simulations and Beji (2019), whereas in Zone II (diffraction-dominated), wave diffraction effects dominate. The Classical Morison equation provides reasonable predictions in turbulent flows despite geometric complexities.

Table 3 provides a detailed comparison of current force results from numerical simulations and predictions from the Morison equations for piles with constant and linearly varying diameters focusing on current cases. The current cases analyzed have the following Reynolds numbers: T1R1 Case 2: $Re = 33825$, T2R3 Case 4: $Re = 22324$, T1R2 Case 6: $Re = 270600$, T2R4 Case 8: $Re = 179272$. All cases (2, 4, 6, and 8) are in the turbulent flow regime. However, Cases 6 and 8 have a much higher Reynolds number, indicating a more intense and fully developed turbulent flow compared to Cases 2 and 4, which are in the turbulent regime but at a relatively lower intensity.

Table 3 Comparative analysis of numerical current force results with classical Morison equation predictions for different pile geometries.

Pile Type	Case	Current	Numerical Force [N]	Classical Morison [N]
T1R1	Case 2	+	1.35	1.25
T2R3	Case 4	+	1.14	1.56
T1R2	Case 6	+	11.07	10.00
T2R4	Case 8	+	12.44	12.63

In T1R1 Case 2, which involves a constant diameter cylinder, the flow is in the turbulent regime. The numerical result for the current force is 1.35 N, while the force calculated using the classical Morison equation is 1.25 N. This shows that the numerical simulation slightly overpredicts the force compared to the semi-empirical formula, suggesting a good but slightly conservative performance of the numerical model in the lower end of the turbulent regime.

In T2R3 Case 4, which features a cylinder with a linearly varying diameter, the Reynolds number suggests a transitional to turbulent flow regime. The numerical result is 1.14 N, significantly lower than the calculated force of 1.56 N from the Morison equation. This discrepancy suggests that the classical Morison equation may not fully account for the complexities of flow around linearly varying diameter piles in a transitional regime. In transitional flow conditions, the flow can exhibit characteristics of both laminar and turbulent regimes, leading to more complex interactions that the classical Morison equation, which assumes a more simplified flow behavior, may not accurately predict. A similar pattern is observed in wave-induced cases like T2R3 Case 3, where the transitional regime also complicates force predictions. Additionally, mesh refinement is particularly important for these cases, given that the piles are slender and require detailed resolution to accurately capture the complex flow patterns.

For T1R2 Case 6, which involves a constant diameter cylinder, the Reynolds number clearly places it within the fully turbulent flow regime. The numerical result is 11.07 N, compared to the 10.00 N calculated using the Morison equation. This overprediction indicates that the numerical model tends to estimate higher forces in high Reynolds number scenarios, possibly due to enhanced turbulence modeling around the large diameter cylinder. A similar overprediction trend is observed in wave-induced cases like T1R2 Case 5, suggesting that the numerical model consistently predicts slightly higher forces in fully turbulent regimes, whether induced by waves or currents, likely due to its detailed turbulence modeling capabilities.

In T2R4 Case 8 (current-induced) and T2R4 Case 7 (wave-induced), both involving cylinders with linearly varying diameters, the Reynolds numbers indicate fully turbulent flow regimes. In Case 8, the numerical force is 12.44 N, while the classical Morison equation predicts a slightly higher force of 12.63 N. This minor discrepancy suggests that, in fully turbulent conditions, the classical Morison equation tends to slightly overpredict the forces on linearly varying diameter piles. A similar trend is observed in the wave-

induced Case 7, where the classical Morison equation also slightly overpredicts compared to numerical results. These consistent findings across both wave and current scenarios indicate that the classical Morison equation still provides reasonable accuracy for fully turbulent flow regimes, despite its simplifications.

The classical Morison equation may not always be adequate for calculating current forces, particularly for structures with complex geometries or in different flow regimes. The differences between the numerical results and the classical Morison equation are more pronounced for the linearly varying diameter pile in the transitional flow regime (Case 4) compared to the constant diameter pile (Case 2). However, for fully turbulent conditions (Case 8), the Morison equation shows a closer match to numerical results, indicating it may be more reliable under these conditions. This suggests that the classical Morison equation's suitability depends on the flow regime and pile geometry. Therefore, the numerical model must be carefully refined, especially near walls and with appropriate mesh refinement, to ensure accurate predictions. This is particularly important for varying diameter piles, where complex flow interactions can lead to significant differences between numerical and semi-empirical results.

6. Conclusions

The novelty of this work lies in focusing on test cases characterized by small Keulegan-Carpenter (KC) numbers and relatively high Reynolds (*Re*) numbers within both inertia-dominated and diffraction zones, where separate waves and currents act on piles with constant and linearly varying diameters. The study includes a thorough analysis of hydrodynamic forces under these conditions, critical in offshore engineering as they represent inertial and turbulent flow systems, respectively.

Simulations have shown that the extended Morison equation provides more accurate force predictions, especially for piles with linearly varying diameters. The results demonstrate that while the classic Morison equation is suitable for constant diameter piles, it fails to capture the complexity of flow interactions around variable diameter piles, resulting in less accurate predictions. In contrast, the extended version of the Morison equation, which includes nonlinear effects and adjustments for variable cross sections, better accounts for these complexities and provides improved predictive capabilities when compared to the classical formulation. This improvement is most significant in the diffraction zone, where the wave structure interaction is particularly complex.

The results emphasize the importance of considering geometric variations and flow patterns in hydrodynamic force calculations. The integration of numerical simulations using RANS equations for validating the extended Morison equation strengthened the reliability of the results. This combined approach not only confirmed the applicability of the extended Morison Equation but also provided practical insights into their application in piles with constant and linearly varying diameters, especially for small KC and high Re numbers. By validating the extended equation against detailed numerical simulations using REEF3D, the study demonstrated the enhanced accuracy and versatility of the extended Morison equation for predicting hydrodynamic forces. However, the observed discrepancies between numerical results and semi-empirical calculations, further underscore the need for careful consideration of grid resolution, particularly to enhance the reliability of turbulence modeling in varying flow regimes. This validation is particularly crucial for modern offshore structures with complex geometries and under specific flow conditions, ensuring more reliable and efficient design and optimization strategies in offshore engineering. Further studies should incorporate experimental validation with a broader range of flow conditions, as well as simulations under the combined action of waves and currents, to enhance the practical applicability of the findings and better reflect the complexities of real marine environments.

REFERENCES

[1]   Sarpkaya, T., 2010. Wave forces on offshore structures. *Cambridge University Press*. https://doi.org/10.1017/CBO9781139195898

[2]   Chakrabarti, S.K. 1987. Hydrodynamics of offshore structures: Mathematical theory and its applications in structures. *Springer-Verlag New York Inc.,* New York, NY.

[3]   Dean, R.G., Dalrymple, R.A., 1991. Water wave mechanics for engineers and scientists, *World Scientific Publishing Company*. https://doi.org/10.1142/9789812385512

[4]   Morison, J.R., Johnson, J.W., Schaaf, S.A., 1950. The force exerted by surface waves on piles. *Journal of Petroleum Technology*, 2, 149-154. https://doi.org/10.2118/950149-G

[5]   Beji, S., 2019. Applications of Morison's equation to circular cylinders of varying cross-sections and truncated forms. *Ocean Engineering*, 187, 106156. https://doi.org/10.1016/j.oceaneng.2019.106156

[6]   Chaplin, J.R., 1984. Nonlinear forces on a horizontal cylinder beneath waves. *Journal of Fluid Mechanics*, 147, 449-464. https://doi.org/10.1017/S0022112084002160

[7]   Ahmed, T.M., Elaghbash, A.O., Banawan, A.A., Ahmed, Y.M., Hassan, A.M., 2020. Numerical prediction of solitary wave formation of a planing hull in shallow water channels. *Brodogradnja*, 71(3), 135-148. https://doi.org/10.21278/brod71308

[8]   Mikulec, M., Piehl, H., 2023. Verification and validation of CFD simulations with full-scale ship speed/power trial data. *Brodogradnja*, 74(1), 41-62. https://doi.org/10.21278/brod74103

[9]   Veić, D., Sulisz, W., Soman, R., 2019. Effect of breaking wave shape on impact load on a monopile structure. *Brodogradnja*, 70(3), 25-42. https://doi.org/10.21278/brod70302

[10]   Avci, A.G., Barlas, B., 2023. Investigation of the optimum longitudinal single transverse step Location for a high-speed craft. *Brodogradnja*, 74(3), 47-70. https://doi.org/10.21278/brod74303

[11]   Zhang, Y., Li, D., Hong, S., Zhang, M., 2023. Design of a new oscillating-buoy type wave energy converter and numerical study on its hydrodynamic performance. *Brodogradnja*, 74(1), 145-168. https://doi.org/10.21278/brod74108

[12]   Clément, C., Bozonnet, P., Vinay, G., Pagnier, P., Nadal, A.B., Réveillon, J., 2022. Evaluation of Morison approach with CFD modelling on a surface-piercing cylinder towards the investigation of FOWT hydrodynamics. *Ocean Engineering*, 251, 111042. https://doi.org/10.1016/j.oceaneng.2022.111042

[13]   Kamath, A., Bihs, H., Alagan Chella, M., Arntsen, Ø.A., 2016. Upstream-cylinder and downstream-cylinder influence on the hydrodynamics of a four-cylinder group. *Journal of Waterway, Port, Coastal, and Ocean Engineering*, 142(4). https://doi.org/10.1061/(ASCE)WW.1943-5460.0000339

[14]   Bihs, H., Chella, M.A., Kamath, A., Arntsen, Ø.A., 2017. Numerical investigation of focused waves and their interaction with a vertical cylinder using REEF3D. *Journal of Offshore Mechanics and Arctic Engineering*, 139(4). https://doi.org/10.1115/1.4036206

[15]   Sathyanarayana, A.H., Suvarna, P.S., Umesh, P., Shirlal, K.G., Bihs, H., Kamath, A. 2022. Numerical modelling of an innovative conical pile head breakwater. *Water,* 14(24), 4087. https://doi.org/10.3390/w14244087

[16]   Bihs, H., Kamath, A., 2016. A combined level set/ghost cell immersed boundary representation for floating body simulations. *International Journal for Numerical Methods in Fluids*, 83(12), 905-916. https://doi.org/10.1002/fld.4333

[17]   Lin, P., Liu, P.L.-F., 1998. A numerical study of breaking waves in the surf zone. *Journal of Fluid Mechanics*, 359, 239-264. https://doi.org/10.1017/S002211209700846X

[18]   Kamath, A., Chella, M.A., Bihs, H., Arntsen, Ø.A., 2015. CFD investigations of wave interaction with a pair of large tandem cylinders. *Ocean Engineering*, 108, 738-748. https://doi.org/10.1016/j.oceaneng.2015.08.049

[19]   Park, M.-S., Koo, W., 2015. Mathematical modeling of partial-porous circular cylinders with water waves. *Mathematical Problems in Engineering*, 903748. https://doi.org/10.1155/2015/903748

[20]   Song, H., Tao, L., Chakrabarti, S., 2010. Modelling of water wave interaction with multiple cylinders of arbitrary shape. *Journal of Computational Physics*, 229(5), 1498-1513. https://doi.org/10.1016/j.jcp.2009.10.041

[21]   Zhao, M., Pengzhen, L., Piguang, W., Chao, Z., Xiuli, D., 2021. An analytical solution for the interaction of waves with arrays of circular cylinders. *Mathematical Problems in Engineering*, 5710894. https://doi.org/10.1155/2021/5710894

[22]   Wang, P., Chang, Y., Zhao, M., Han, J., 2020. Earthquake and wave analysis of circular cylinder considering water-structure-soil interaction. *Advances in Civil Engineering*, 4271378. https://doi.org/10.1155/2020/4271378

[23]   Ghadirian, A., Vested, M.H., Carstensen, S., Christiensen, E.D., Bredmose, H., 2021. Wave-current interaction effects on waves and their loads on a vertical cylinder. *Coastal Engineering*, 165, 103832. https://doi.org/10.1016/j.coastaleng.2020.103832

[24]   Isaacson Michael de St.Q., 1979. Nonlinear inertia forces on bodies. *Journal of the Waterway, Port, Coastal and Ocean Division*, 105(3), 213-227. https://doi.org/10.1061/JWPCDX.0000150

[25] Koterayama, W., Hu, C., 1995. Wave forces on horizontal cylinders at low Keulegan-Carpenter and Reynolds Numbers. *5th International Offshore and Polar Engineering Conference*, 11-16 June, The Hague, Netherlands.

[26] Aksel, M., Yagci, O., Kirca, V.S.O., Erdog, E., Heidari, N., 2021. A comparative analysis of coherent structures around a pile over rigid-bed and scoured-bottom. *Ocean Engineering*, 226, 108759. https://doi.org/10.1016/j.oceaneng.2021.108759

[27] Kitsikoudis, V., Yagci, O., Kirca, V.S.O., Kellecioglu, D., 2016. Experimental investigation of channel flow through idealized isolated tree-like vegetation. *Environmental Fluid Mechanics*, 16(6), 1283-1308. https://doi.org/10.1007/s10652-016-9487-7